Journal of Materials Chemistry B

PAPER

Check for updates

Near-infrared light-mediated and nitric oxide-supplied nanospheres for enhanced synergistic thermo-chemotherapy†

Chuan Zhang,[a] Qiqing Li,[b] Yue Zhao,[a] Hou Liu,[a] Shanliang Song,[a] Yueqi Zhao,[a] Quan Lin [ID] *[a] and Yulei Chang [ID] *[b]

Synergistic thermo-chemotherapy based multiple stimuli-responsive drug delivery systems have achieved significant improvement of cancer curative effects compared with single modality treatment. Nevertheless, the efficacy of thermo-chemotherapy is often reduced in drug-resistant tumors and the therapy method is unexpectedly associated with potential toxicity by utilizing poorly degradable materials. Here, we report a simple approach to encapsulate three drug payloads into multi-sensitive and degradable nanospheres (SDC@NS) to achieve anticancer effects. SDC@NS comprise a photothermal agent (cypate), an anticancer agent (doxorubicin), and a nitric oxide donor (SNAP) to achieve controllable drugs release in high concentration glutathione or under near-infrared light (NIR) irradiation. Hyperthermia from NIR-mediated cypate can accelerate cancer cell apoptosis *in vitro* and tumor tissue ablation *in vivo*. Furthermore, our results also confirmed that the nitric oxide-based SDC@NS showed significant cytotoxicity compared to the nitric oxide absent group (denoted as DC@NS) and an enhanced chemotherapy effect *in vivo*. The photothermal effect and payloads can synchronously realize cancer therapy and provide a new insight into the enhanced synergistic therapeutic effect.

1. Introduction

In recent years, multiple stimuli-responsive drug delivery systems (MSDDS) have been considered as one of the promising cancer therapy strategies to overcome the difficulties of chemotherapeutic drugs in serious toxic side effects, low efficiency, fast clearance, *etc.*[1–5] Generally, MSDDS responding to pH, redox, and temperature can quickly release payloads and effectively elevate the curative effect against cancer.[6–8] To further improve the treatment efficacy of MSDDS, researchers combine MSDDS with other therapy methods, such as radiotherapy, photothermal therapy, and convenient surgery. Among them, MSDDS-based thermal-chemotherapy can accomplish efficient cancer therapy with the help of chemotherapeutic drugs and photothermal agents.[9–11] The resulting local hyperthermia from the thermal-chemotherapy platform can increase membrane permeability and cellular metabolism for enhancing the uptake of drugs by cells, which improves the utilization of chemotherapeutic drugs, as well as causing heat

damage to cancer cells.[12] Although the MSDDS possess excellent capabilities to respond to external stimuli, their thermo-chemotherapy efficacy will be greatly reduced in drug-resistant tumors, losing its associativity and hindering further application in cancer therapy.[13–15] Therefore, to address this problem, the overcoming drug resistance elements should be contained in the desirable thermo-chemotherapy system.[16–18]

Notably, nitric oxide (NO) is a water-soluble, lipophilic, highly diffusible free radical gas that exerts necessary physiological and pathophysiological functions and plays a potential anti-oncogenic role in cells.[19,20] Based on its anti-oncogenic properties, NO is used as an emerging adjuvant chemotherapy agent to get an excellent anticancer efficacy, which generally induces DNA cleavage and toxic effects on membrane proteins by oxidation or nitrosation at high concentrations.[21–23] It also acts as a vasodilator to promote cancer cell infiltration and proliferation at low concentrations.[24] Considering the double physiological influence of NO, the dose-controllable NO release systems have outstanding advantages and attract extensive interest in precise NO release by tuning the external signals (*e.g.*, light, heat and heavy metals).[25,26] It is delightful to know that the photothermal effect not only damages cancer tissues but also triggers NO release from thermal-responsive NO prodrugs. Thus, researchers had developed some NO delivery systems combining multi-stimuli responsive vehicles with the photothermal agents. In most of the NO generation

a State Key Laboratory of Supramolecular Structure and Materials, College of Chemistry, Jilin University, Changchun, 130012, P. R. China. E-mail: linquan@jlu.edu.cn

b State Key Laboratory of Luminescence and Applications, Changchun Institute of Optics, Fine Mechanics and Physics, Chinese Academy of Sciences, Changchun, Jilin 130033, China. E-mail: yuleichang@ciomp.ac.cn

† Electronic supplementary information (ESI) available. See DOI: 10.1039/c8tb02939c

548 | *J. Mater. Chem. B*, 2019, **7**, 548–555

This journal is © The Royal Society of Chemistry 2019

nanovehicles, hardly biodegradable materials (graphene oxide, quantum dots, nanocrystals, and upconversion nanoparticles) were used as photoactive carriers that absorb NIR photons and accelerated NO release, but these approaches could not display chemotherapeutic assistance, thereby posing a low efficient problem.[27–33] Moreover, in several studies, heavy metal-functionalized NO donors had been introduced into NO-releasing systems, and such heavy metal-related nanoparticles generally suffered from potential toxicity in biological application.[29,34]

In this work, we developed multi-sensitive biodegradable nanospheres (SDC@NS) for anticancer applications in synergistic thermo-chemotherapy, loaded with cypate, doxorubicin (DOX), and S-nitroso-N-acetyl-D,L-penicillamine (SNAP, a kind of NO donor). Because the concentration of glutathione (GSH) in the tumor cytosol was several times higher than that in the normal cells, the GSH-cleavable ability of cross-linked networks in SDC@NS could achieve accelerative drug release.[35] Meanwhile, when the temperature of SDC@NS was higher than volume-phase-transition temperature (VPTT), the drug release behavior was also accelerated by polymer shrinkage.[36] As illustrated in Scheme 1, the obtained nanospheres presented an enhanced DOX release behavior, responding to glutathione (GSH) and NIR-mediated hyperthermia. Hyperthermia also exhibited accelerative NO generation because it could cleave the S–NO bond of SNAP to form NO molecules. These capsuled drugs in the as-designed SDC@NS mainly exerted the synergistic anticancer effect in three aspects: firstly, cypate converted NIR energy into hyperthermia, which synchronously accelerated drug release and induced cancer cell apoptosis. Secondly, DOX interfered with the synthesis of DNA

by inserting the double-stranded base pairs of DNA and uniting with nucleic acid.[37] Furthermore, NO induced DNA damage and enzyme inhibition in cancer cells. Our study presented a novel strategy for expanding NO application and enhancing synergistic thermal-chemotherapy, showing great potential for future clinical application. The combination of DOX and NO can both interfere with the synthesis of DNA and damage DNA, and the photo-thermal effect can damage cancer cells, realizing cancer therapy and an enhanced therapeutic effect.

2. Materials and methods

2.1. Materials

N,N'-Bis(acryloyl)cystamine (BAC), N-isopropyl acrylamide (NIPAM), glutathione (GSH), and S-nitroso-N-acetyl-D,L-penicillamine (SNAP) were purchased from J&K. Diethylene triamine pentaacetic acid (DTPA) and 2-acrylamido-2-methyl propane sulfonic acid (AMPS) were purchased from Aladdin. Doxorubicin hydrochloride (DOX·HCl) was provided by Dalian Meilun Biotechnology Co., Ltd. The nitric oxide assay kit was obtained from Beyotime Biotechnology Co., Ltd. DAPI and DAF-FM DA were all obtained from Beijing biorab Technology Co. Ltd. Cypate was synthesized referring to the previous work.[38] Other solvents and compounds were purchased from Beijing Chemical Works and used without further purification.

2.2. Preparation of PNIPAM-SS-AMPS nanospheres

Multi-sensitive nanospheres (NS) were synthesized by emulsion polymerization.[39,40] Briefly, calculated amounts of NIPAM, AMPS, and cross-linker BAC with the corresponding feeding weight ratio of 22 : 3.2 : 1 were added into a three-necked round-bottom flask and dissolved in 185 mL deionized water. Then, 0.04 wt% of SDS was added as a surfactant. The above mixture was stirred (400 r min^{-1}) under a nitrogen (N$_2$) atmosphere at room temperature for 30 min to remove oxygen and then heated to 70 °C. Afterward, 15 mL of KPS aqueous solution (10 mg mL^{-1}) was added to initiate polymerization. The reaction mixture was kept at 70 °C for 12 h. The resulting nanospheres were dialyzed in a dialysis membrane (MW cut-off 14 000) against Di-water for 2 days and then lyophilized to obtain the nanospheres for further use.

2.3. Preparation of DOX-cypate-loaded nanospheres (DC@NS)

To encapsulate cypate, a dialysis method was employed. First, 2 mg of cypate was dissolved in 1 mL of methanol, and then 5 mL of the nanosphere aqueous (2 mg mL^{-1}) was gradually dropped into the cypate solution. The mixture was dialyzed against water for 3 days to remove methanol and then the solvent was evaporated to keep a constant concentration of nanospheres. Subsequently, 2 mg of DOX·HCl was dispersed in 2 mL PBS under ultrasonic oscillation. The DOX suspension was then dropped into the NS mixture. Then, the mixture was stirred for 12 h at room temperature in the dark. DC@NS were purified using a filter under reduced pressure and then lyophilized to obtain DC@NS for further use.
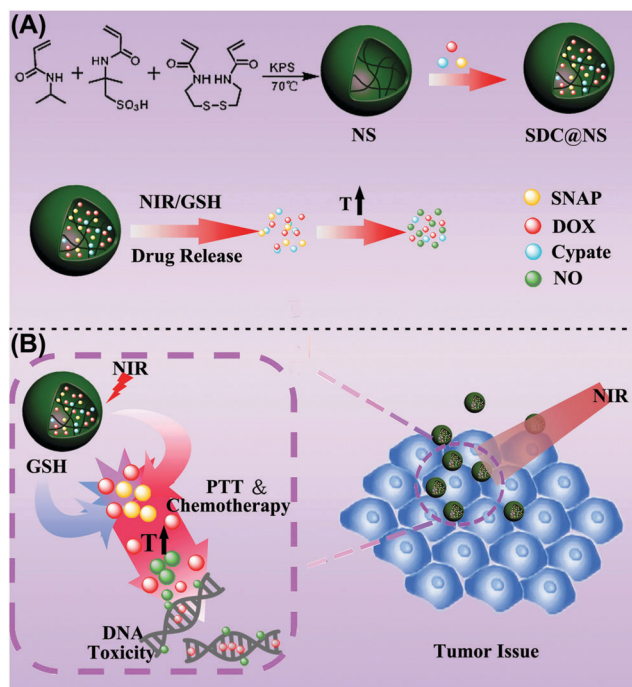
Scheme 1 (A) Construction of SDC@NS and drug release behavior and (B) schematic illustration of NIR light-induced synergistic thermo-chemotherapy and DNA damage.

2.4. Preparation of SNAP-DOX-cypate-loaded nanospheres (SDC@NS)

The preparation method of SDC@NS was similar to that of DC@NS. Briefly, 2 mL of a DC@NS aqueous solution (4 mg mL^{-1}) containing 100 µM DTPA was stirred at 0 °C in a dark environment. Then, 1 mg of SNAP was added and then stirring was continued for 3 h. SDC@NS were obtained and purified using a syringe filter. The concentrations of SNAP, DOX, and cypate in the nanospheres were measured by UV-Vis spectroscopy (TU-1991 UV-Vis) at 340, 480 and 786 nm, respectively. The hydrodynamic diameter and zeta potential of SDC@NS were measured by dynamic light scattering (DLS, Zetasizer Nano ZS). The morphology of SDC@NS was detected by transmission electron microscopy (TEM, JEM-2100). Loading efficiency (wt%) = (mass of drugs in the carriers)/(mass of carriers loaded with drugs).

2.5. In vitro photothermal effect

To study the photothermal effect, the photothermal conversion performances of SDC@NS aqueous dispersions with various cypate concentrations (0, 2, 5, 10, 15, and 25 µg mL^{-1}) were measured under 808 nm laser irradiation (1 W cm^{-2}) within 5 min. On the basis of the above results, 10 µg mL^{-1} of cypate at different pH (5.0, 7.4 and 8.0) buffer solutions were used to study the photothermal conversion properties in simulated normal tissues and tumor tissues. The internal temperature changes of the sample were monitored using a thermocouple thermometer. Meanwhile, the equipotent cypate concentration of SDC@NS was measured under the same conditions and the PBS solution as a control. The light-induced temperature changes were monitored using a FLIR E50 Infrared (IR) camera.

2.6. GSH and NIR light-responsive DOX release studies

The DOX release behaviors were determined by the dialysis method under different conditions including GSH and NIR light. Briefly, 2 mL of the SDC@NS solution (4 mg mL^{-1}) was added in 8 mL of phosphate buffer solution containing different concentrations of GSH at 37 °C. The solution was transferred to the dialysis bag against PBS buffer solution of pH 7.4. Fresh PBS buffer solution replaced the external fluid membrane at the indicated time points. For NIR light-mediated DOX release, a similar procedure was performed in addition to 808 nm laser irradiation (1 W cm^{-2}) for 5 min. The concentrations of DOX were determined by UV-Vis spectroscopy (TU-1991 UV-Vis) at 480 nm.

2.7. NIR light-controlled release of NO

The NO release behaviors were determined by Griess assay.[20] In brief, 6 mL of SDC@NS (4 mg mL^{-1}) solution containing 100 µM DTPA were stirred in a dark environment. After exposure to a NIR laser (808 nm, 1 W cm^{-2}) for 10 min at a time point of 0.5 h, 0.5 mL of SDC@NS solution was extracted to measure the absorption at 541 nm and further diluted to 2 mL by the Griess solution. Immediately, the concentrations of the NO in the diluent were measured using UV-Vis spectroscopy (TU-1991 UV-Vis) at 541 nm.

2.8. Cell culture and cellular uptake of the nanospheres

MCF-7/ADR cells were obtained from Cancer Hospital of Jilin Province, Jilin, China. Cell culture related supplies were purchased from NEST Biotechnology and reagents were obtained from Invitrogen. MCF-7/ADR cells were cultured with RPMI 1640 supplemented with 10% fetal bovine in a 5% CO$_2$ humidified atmosphere at 37 °C.

The cellular uptake of SDC@NS was monitored via CLSM. MCF-7/ADR cells (1 × 10^5) were grown in a glass bottom cell culture dish at 37 °C for 24 h. Then 30 µL of SDC@NS solution was added to the medium. The DOX fluorescence of samples was observed by CLSM at designed time points (1, 2, 4 and 6 h).

In vitro controllable drug release of SDC@NS was carried out under NIR irradiation or at high concentration of GSH. Briefly, MCF-7/ADR cells were incubated with RPMI 1640 medium containing 10 mM of GSH at 37 °C for 24 h. Then 30 µL of SDC@NS solution was added to the MCF-7/ADR cells and the cells were irradiated (808 nm, 1 W cm^{-2}) for 5 min. The cells were stained for 20 min with DAPI. All the samples were incubated for 1 h and the DOX fluorescence of samples was observed by CLSM.

2.9. Intracellular NO release detection

MCF-7/ADR cells (1 × 10^5) were seeded in a glass bottom cell culture dish and cultured overnight. Then 30 µL of SDC@NS were incubated with cells for 4 h at 37 °C. After replacing with fresh culture media, 10 µL of DAF-FM DA were loaded with cells in RPMI 1640 medium for 20 min at 37 °C. Subsequently, the cells were irradiated (808 nm, 1 W cm^{-2}) for 5 min followed by rinsing of culture medium three times. The DAF-FM DA fluorescence of each sample was observed immediately at 515 nm (excitation at 495 nm) by CLSM.

2.10. In vitro cytotoxicity of the nanospheres

The cytotoxicity of nanospheres was assessed by MTT assays. The MCF-7/ADR cells were seeded in 96-well plates at a density of 5000 cells per well. After incubation for 24 h, different doses of drug loaded nanospheres were incubated with cells and the blank nanospheres were incubated for another 24 h at 37 °C. To study the phototoxicity of nanospheres, the cells were irradiated with a NIR laser (808 nm, 1 W cm^{-2}) for 5 min after 4 h incubation. After another 20 h incubation, the cell viability was determined by a standard MTT assay. The absorbance at 490 nm was measured using a microplate reader.

2.11. In vivo photothermal effect IR imaging and therapy

For in vivo photothermal IR imaging and therapy of SDC@NS, xenograft tumors were established by inoculating the C57BL/6 mice with LLC cell lines. When the tumors reached around a volume of 50 mm^3, therapeutic agents for in vivo antitumor efficacy measurements, LLC xenograft mice were randomly assigned to four groups (n = 3 per group). The tumor volumes were measured using a caliper every two days and calculated using the formula: $1/2 \times a \times b^2$, where a and b are the largest and the smallest diameters, respectively. The mice were injected

550 | J. Mater. Chem. B, 2019, 7, 548–555

This journal is © The Royal Society of Chemistry 2019

with DOX doses of 5 mg kg^{-1} for every test group, respectively, PBS as a control group. Therapeutic agents were intravenously injected on 4, 6, and 8 d, respectively. The NIR-treated groups were irradiated with an 808 nm laser (1 W cm^{-2}, 3 min) at 5 h post-injection. Additionally, the tumor tissue was irradiated for 5 min by a NIR laser (808 nm, 1 W cm^{-2}), and the temperature change of the tumor was observed using an IR camera, simultaneously. All the animal experiments were approved by the Animal Care Committee of Jilin University and conformed to the Animal Ethical Standards and Use Committee at Jilin University.

3. Results and discussion

3.1. Synthesis and characterization of SDC@NS

The multi-responsive nanospheres were synthesized via emulsion polymerization using N-isopropylacrylamide (NIPAM) and 2-acrylamido-2-methyl propane sulfonic acid (AMPS) as monomers and N,N'-bis(acryloyl)cystamine (BAC) as the glutathione (GSH) sensitive cross-linker. NIPAM endowed nanospheres with heat-mediated volume shrink ability and AMPS was chosen to maintain the stability of nanospheres during the long circulation time in the physiological environment. Cypate, doxorubicin, and S-nitroso-N-acetyl-D,L-penicillamine (SNAP) were loaded into nanospheres step by step with a drug loading efficiency of 8.63%, 5.24%, and 7.69%, respectively (Fig. S3, ESI†). As shown in Fig. 1A, uniformly spherical nano-sized structures with a mean diameter of 92.2 nm were revealed by TEM imaging. The main size of SDC@NS was about 125.5 nm in PBS solution by DLS analysis and the polydispersity index (PDI) was 0.114, exhibiting a narrow size distribution and good aqueous dispersion. The sizes of blank nanospheres by TEM and DLS were about 110 nm and 252.9 nm (Fig. S1, ESI†), these changes compared to the SDC@NS might be related to the hydrophobic interaction between drugs and nanospheres. The hydrodynamic size of nanospheres was larger than that observed by TEM relatively because of the shrink effect of nanospheres under dry conditions. As depicted in Fig. 1B, the zeta potential of nanospheres was −5.4 mV in a simulant cancer environment (pH = 5.0) and

−6.1 mV under normal physiological conditions (pH = 7.4). The zeta potential results indicated that nanospheres with negative charge possessed the stability, combining hardly with negative charge substances in blood, body fluid, and the cell membrane. It ensured the stability of releasing payloads in the acidic tumor tissue. Furthermore, the volume phase transition temperature (VPTT) was another key parameter of temperature-sensitive nanospheres related to carrier stability and drug release behavior under physiological conditions. At this temperature, the PNIPAM segments faced a phase transition from fully hydrated chains to hydrophobic. Regulating the VPTT at physiological temperature (∼37 °C) could partly reduce drug leakage during the circulation process and accelerate drug release upon NIR light irradiation.[36] As shown in Fig. 1C, AMPS in the polymer chain structure of nanospheres had an important effect on the volume-phase transition behavior: the hydrophilic AMPS monomer (feeding rate of 7.5 wt%, see Table S1, ESI†) could adjust the VPTT of nanospheres to 37.8 °C, ensuring circulation stability of nanospheres under physiological conditions and rapid release of payloads under hyperthermia conditions. Fig. 1D shows the absorption spectra of drugs and nanospheres dispersed in PBS. Previous works had confirmed a DOX absorption peak at 480 nm.[10] Cypate and SNAP exhibited an absorption peak at 786 nm and 340 nm, respectively. In the absorption curve of SDC@NS, obvious absorption peaks appeared at 340 nm, 480 nm and 786 nm. Moreover, in the near infrared region a strong broad absorption peak with a slight red-shift (from 786 nm to 791 nm) appeared, probably due to the J-aggregation effect of cypate. This red shift phenomenon can enhance absorption of cypate at 808 nm and improve its photothermal conversion capability to achieve PTT.[41]

3.2. Photophysical properties of nanospheres

To demonstrate the photothermal effect of SDC@NS, we studied the generation of hyperthermia. As depicted in Fig. 2A, the SDC@NS exhibited remarkable temperature elevation (ΔT) upon NIR exposure (808 nm, 1 W cm^{-2}, 300 s), ranging from 3.2 to 17.9 °C in the
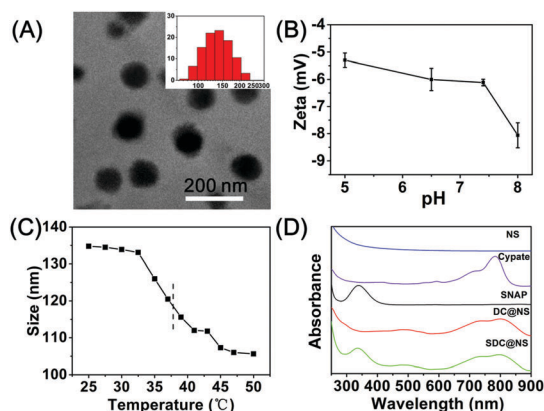

Fig. 1 (A) TEM image and size distribution of SDC@NS. (B) Zeta potential of SDC@NS at various pH values. (C) Hydrodynamic size of SDC@NS at different temperatures. (D) Absorbance spectra of nanospheres, cypate, SNAP, DC@NS, and SDC@NS in aqueous solution.
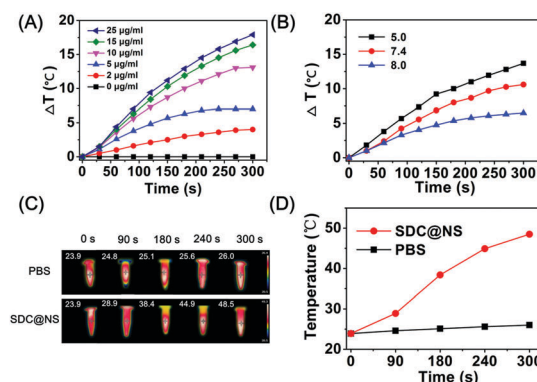

Fig. 2 (A) Temperature change of SDC@NS containing various cypate concentrations at different time points under NIR irradiation. (B) Temperature elevation of SDC@NS containing 10 μg mL^{-1} cypate at different pH values. (C) Temperature images of 10 μg mL^{-1} cypate at different time points under NIR irradiation recorded using an IR camera. (D) Temperature curves of the IR image groups.

cypate concentration range of 2–25 µg mL^{-1}. Whereas the PBS control group only induced a negligible increase in temperature. These results reveal that the NIR-mediated evaluation behaviour of cypate is concentration-dependent. Accordingly, the infrared thermal images of SDC@NS aqueous solution with the same concentration were obtained (Fig. 2C and D), the surface temperature of samples exhibited a rapid increase in the SDC@NS group, compared with unconspicuous temperature elevation in the PBS group. Moreover, the photothermal effect of SDC@NS was enhanced in the acidic environment (Fig. 2B). Compared to pH of 7.4 and 8.0, a faster temperature elevation was obtained upon 300 s irradiation in a pH = 5.0 solution containing 10 µg mL^{-1} of cypate. This phenomenon was attributed to nonradiative transition enhancing the photothermal effect in the acidic environment.[42] These results indicate that the rapid enhancement photothermal effect of SDC@NS can easily generate hyperthermia (>45 °C) to damage tumor cells especially in the acidic subcellular organelles such as *endo-/lysosome* by the endocytosis mechanism.[42] This photothermal effect not only guarantees the PTT effect of the tumor but also acts as a pivotal condition to ensure that the nanosphere volume shrinks in favor of the drug release.

3.3. GSH and NIR light-responsive drug release

The drug release profiles of SDC@NS were studied under the simulated normal physiological conditions and in a tumor tissue environment with different stimuli. Firstly, the DOX release behavior was studied in PBS (pH = 7.4) solution with variable GSH concentrations (Fig. 3A). The cumulative release of DOX without GSH was 15% in 2 h and 30% in 24 h respectively. The phenomenon could be explained that the adsorptive DOX in the hydrophilic nanosphere shell could release rapidly and the encapsulated DOX released slowly, because of the hydrophobic interaction between the DOX and cross-linked network. After introducing 10 mM and 30 mM of GSH into PBS, DOX release reached 24% and 63% in 2 h, respectively, and the accumulative release amount obviously accelerated as high as 60% and 90%, which was attributed to the cleavage of the disulfide bond of the cross-linked network by reductive GSH and decline of hydrophobic interaction between DOX and polymer chains.

Next, the NIR light-mediated drug release profile was studied. In the presence of 10 mM GSH, SDC@NS led to significantly increased release of DOX upon NIR light irradiation compared to the NIR absent group. As shown in Fig. 3B, upon momentary NIR irradiation (808 nm, 1 W cm^{-2}, 5 min) exposed to SDC@NS at sampling times of 1 h and 2 h, 11% and 30% DOX release exaltation was obviously observed at the next sampling time (1.5 h and 3 h) compared to no NIR light exposure. After removing light irradiation, the DOX release velocity tended to be steady and the accumulative release returned back to slow growth. It demonstrates that cypate possesses a significant photothermal conversion property in response to NIR irradiation, resulting in enhanced DOX release during the nanosphere phase-transition.

Furthermore, the Griess assay was employed to investigate the NO release profiles from the SDC@NS under NIR light irradiation. As shown in Fig. 3C, after 10 min exposure of 808 nm NIR light at 1 W cm^{-2}, 54.5% of NO was immediately generated and the accumulative NO release reached 91.0% within 4 h, in contrast, only 26.7% of NO was produced within 4 h in the dark group. It indicated that hyperthermia promoted the cleavage of the S–NO bond of SNAP and rapidly released NO. Our results demonstrate that the NO release behavior can be well controlled by the NIR laser stimulus on demand, which is of great significance to reduce the risk of NO poisoning and manipulate the chemotherapy effect within the therapeutic window.

3.4. Cellular uptake of the nanospheres and controllable drug release *in vitro*

To visualize the cellular uptake of the nanospheres, MCF-7/ADR cells were incubated with SDC@NS for 1, 2, 4 and 6 h at 37 °C with an equivalent drug concentration and further imaged by CLSM. The localization of the cell nucleus was confirmed by DAPI with the blue fluorescence and the red fluorescence was from DOX. As illustrated in Fig. S4 (ESI†), after incubation with SDC@NS for 1 h, weak red fluorescence in the cytoplasm could be observed, which indicated that SDC@NS were taken up by MCF-7/ADR cells through endocytosis. Then the red fluorescence was gradually enhanced with incubation time extension until no obvious enhancement of the fluorescence signal at 6 h. In particular, the intensity of red fluorescence in the nucleus was higher than in the cytoplasm obviously in 4 h and 6 h, because DOX primarily acts on the DNA of the nucleus further inhibiting its reproduction.[25]

Furthermore, the stimuli-responsive release of DOX from SDC@NS was studied after 1 h incubation with MCF-7/ADR.
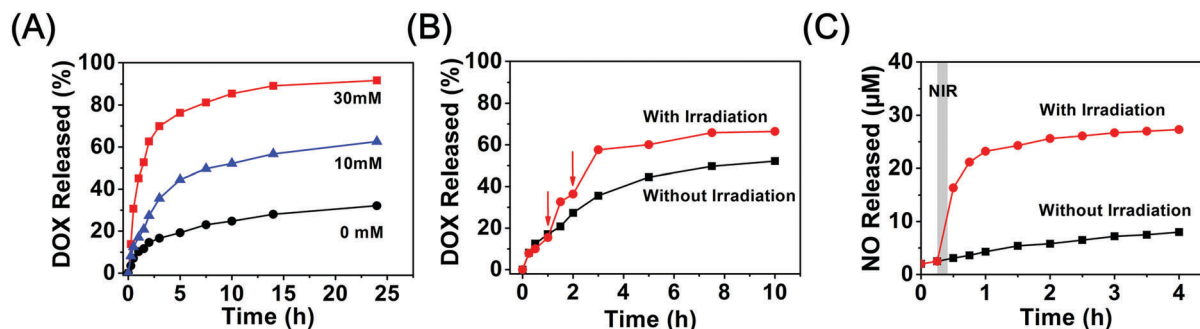

Fig. 3 (A) Accumulative release profiles of DOX from SDC@NS at different concentrations of GSH. (B) Accumulative release profiles of DOX from SDC@NS at 10 mM of GSH with or without NIR irradiation. (C) The on/off generation of NO upon NIR laser irradiation.
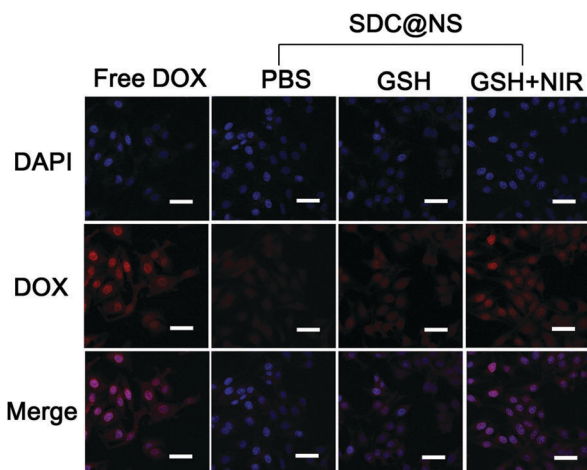
552 | *J. Mater. Chem. B*, 2019, 7, 548–555

This journal is © The Royal Society of Chemistry 2019

Fig. 4 CLSM images of MCF-7/ADR cells after incubation for 1 h with free DOX and SDC@NS (in the presence or absence of GSH or NIR). The scale bars correspond to 50 μm in all the images.

As shown in Fig. 4, bright red fluorescence in the nucleus is clearly observed in the free DOX group, due to its cell membrane penetration capability and the effect of complex formation with DNA. The bright red fluorescence in the free DOX group was related to the rapid cellular uptake, which would induce the fast clearance and frequent dosing *in vivo*. In contrast, various degrees of weak fluorescence can be seen in the other three groups, attributed to the slow and controllable DOX release from drug vehicles. Comparing fluorescence intensity among the groups of PBS, GSH, and GSH + NIR, an obvious fluorescence enhancement appeared in the GSH + NIR group, indicating that intracellular DOX accumulative release is controllable by modulating NIR light-mediated hyperthermia and concentration of the reductive GSH. These results further confirm that SDC@NS can rapidly and sensitively respond to temperature or GSH, promising for a satisfying synergistic thermo-chemotherapy.

3.5. Controlled release and detection of NO

Intracellular NO triggered release from SDC@NS was measured using a DAF-FM DA fluorescence probe in MCF-7/ADR cells. The MCF-7/ADR cells were cultured with SDC@NS or PBS for 4 h before NIR light irradiation. As illustrated in Fig. 5, a very
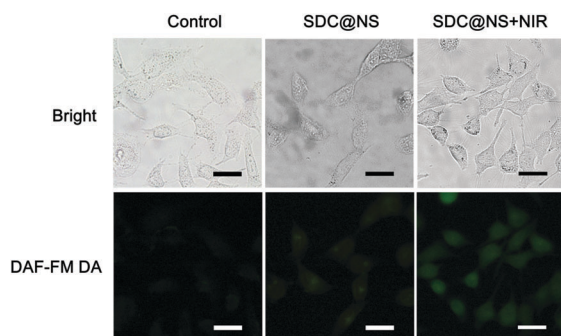
weak green fluorescence signal of DAF-FM DA could be observed in the control group, indicating that traces of NO in living cells maintained physiological metabolic balance. Meanwhile, a negligible fluorescence signal was observed in SDC@NS with the absence of NIR light irradiation, due to the sustained generation of NO in the intracellular environment. Correspondingly, a much stronger fluorescence signal was observed in SDC@NS with the presence of NIR light irradiation, deriving from the generation of an enormous amount of NO upon NIR irradiation for short intervals. The intracellular NO with high concentration will break the metabolic balance of NO and form reactive nitrogen species through a series of physiological actions, including $^{\bullet}OONO$, $^{\bullet}NO_2$, $^{\bullet}NO$ *etc.*, which will cause DNA damage, enzyme inactivation and suppression of the DNA repair system to promote cell apoptosis.[25] These results indicate that SDC@NS are an excellent NO delivery system for NIR-mediated NO release and have the potential for use in NO-enhanced thermal-chemotherapy.

3.6. *In vitro* cytotoxicity of the nanospheres

The therapeutic efficacy of the as-prepared nanospheres was checked by the MTT assay. Fig. S5 (ESI†) shows the relative viability of MCF-7/ADR cells incubated with 0–2 mg mL^{-1} of blank NS in 24 h. Although the highest concentration of blank NS reached 2 mg mL^{-1}, the viability of MCF-7/ADR cells was about 89%. This result proves that the blank NS was hypotoxic. As shown in Fig. 6, the cell viability of the NIR treated group was lower than that of only DOX-loaded DC@NS, due to the fact that hyperthermia from NIR energy transform could down-regulate enzyme activity and even provoke enzyme inactivation by the thermal effect. In addition, when cells were treated with a low drug concentration (0.25 μg mL^{-1}), the groups of SDC@NS plus NIR irradiation had the enhanced effect on cell-killing compared with the groups treated only with DC@NS or DC@NS plus NIR light irradiation. With the increase of drug concentration, the cell viability treated with SDC@NS plus NIR irradiation groups showed a significantly decreased trend than those containing only DC@NS and DC@NS plus NIR irradiation groups. Comparison between the NIR irradiation groups of SDC@NS and DC@NG showed that the former showed lower
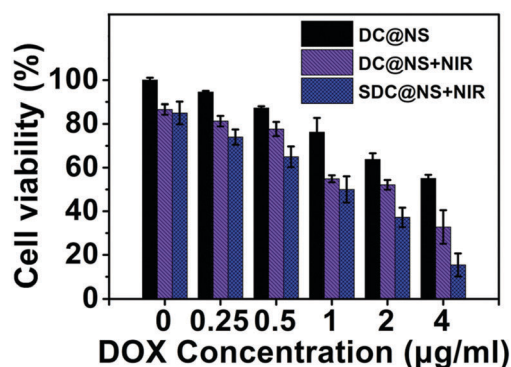

Fig. 5 CLSM images of MCF-7/ADR cells after incubation for 4 h with SDC@NS in the presence of NIR. The generation of NO was detected by DAF-FM DA. The scale bars correspond to 30 μm in all the images.

Fig. 6 Cell viability of MCF-7/ADR cells treated with DC@NS or SDC@NS for 24 h at various concentrations in the dark and 1 W cm^{-2} irradiation (808 nm, 5 min).
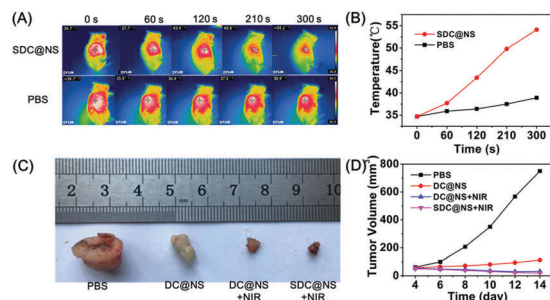
Fig. 7 (A) *In vivo* photothermal effects of SDC@NS. (B) Temperature curves of the NIR irradiated groups corresponding to (A). (C) Photographs of *ex vivo* tumor tissue after 14 day treatment. (D) Corresponding tumor inhibition rate recorded after administration from 4 to 14 days.

cell viability, indicating that NO had an inhibitory effect on MCF-7/ADR cells. These results demonstrate that large-dose NO is capable of killing cancer cells and a higher killing efficacy is achieved as the rapidly released NO and DOX exert a combined effect on cancer cells.

3.7. *In vivo* photothermal effect IR imaging and therapy

In order to evaluate the photothermal effect ability of SDC@NS *in vivo*, NIR-triggered photothermal imaging in tumor tissues was monitored using an 808 nm laser (1 W cm^{-2}) after 5 h post-injection. As depicted in Fig. 7A and B, after tail vein injection with 100 μL of PBS and SDC@NS, we recorded the surface temperature change in the tumor area with various irradiation times. The PBS group exhibited a slight temperature increase (from 34.7 to 38.9 °C) within 300 s irradiation. At this temperature it is difficult to destroy tumor issues and tolerated by the normal organization. The SDC@NS group achieved a significant temperature increase at the tumor site (from 34.7 to 54.1 °C) under the same irradiation conditions, inducing irreversible cancer cell damage.[42] These data reveal that SDC@NS exhibit an excellent ability to achieve precise cancer thermal therapy.

The volume of *ex vivo* tumor after the SDC@NS + NIR synergistic therapy shown in Fig. 7C and the tumor volumes of mice were measured every two days during the therapy process (Fig. 7D). As compared with the PBS injected group, the tumor treated with DC@NS alone was only partially suppressed, demonstrating that the simple chemotherapy was insufficient to inhibit tumor growth *in vivo*. In sharp contrast, the tumor volume on DC@NS and SDC@NS treated groups under NIR laser irradiation was significantly decreased over the whole therapy process. By comparing the DC@NS and SDC@NS groups under NIR laser irradiation, a slightly advantageous inhibitory effect could be observed *in vivo*. Accordingly, the tumor treated with SDC@NS under NIR laser irradiation was the smallest in all groups, confirming highly effective therapy efficacy of the combined photothermal-chemotherapy.

4. Conclusions

In summary, we constructed multi-responsive nanospheres with enhanced thermo-chemotherapy by combining with therapeutic

agents of cypate, DOX, and SNAP. The nanospheres were synthesized *via* emulsion polymerization and obtained with narrow size distribution and good aqueous dispersion. The well-defined SDC@NS could efficiently release the payloads through their decomposition and fast phase transition, triggered by both reductive GSH and NIR-mediated hyperthermia, respectively. Besides, the employed NIR light further enhanced the intracellular drug accumulation to achieve apoptosis. Combination of NO with DOX also accelerated the apoptosis of MCF-7/ADR cells by improved DNA toxicity and enzyme inhibition. SDC@NS therapy *in vivo* results confirmed that it could combine thermo-chemotherapy to achieve effective therapy efficacy and a slightly advantageous inhibitory effect could be observed in the presence of NO. In our design, the proposed NO-generating multi-responsive nanospheres have profound significance for enhanced synergistic thermo-chemotherapy, and it may provide a new strategy with a consensus on synergistic cancer therapy.

Conflicts of interest

There are no conflicts to declare.

Notes and references

1 X. An, A. Zhu, H. Luo, H. Ke, H. Chen and Y. Zhao, *ACS Nano*, 2016, **10**, 5947–5958.
2 Y. Fang, W. Yang, L. Cheng, F. Meng, J. Zhang and Z. Zhong, *Acta Biomater.*, 2017, **64**, 323–333.
3 J. Lee, D.-H. Kim, K. J. Lee, I. H. Seo, S. H. Park, E. H. Jang, Y. Park, Y.-N. Youn and W. Ryu, *J. Controlled Release*, 2017, **268**, 237–246.
4 K. Zhang, H. Chen, F. Li, Q. Wang, S. Zheng, H. Xu, M. Ma, X. Jia, Y. Chen, J. Mou, X. Wang and J. Shi, *Biomaterials*, 2014, **35**, 5875–5885.
5 S. Kumar-Krishnan, M. Guadalupe-Ferreira García, E. Prokhorov, M. Estevez-González, R. Pérez, R. Esparza and M. Meyyappan, *J. Mater. Chem. B*, 2017, **5**, 7072–7081.
6 J. Li, Y. J. Ma, Y. Wang, B. Z. Chen, X. D. Guo and C. Y. Zhang, *Chem. Eng. J.*, 2018, **341**, 450–461.
7 Y. Pan, H. Xiao, P. Cai and M. Colpitts, *Carbohydr. Polym.*, 2016, **135**, 94–100.
8 J. Qu, Q.-y. Wang, K.-l. Chen, J.-b. Luo, Q.-h. Zhou and J. Lin, *Colloids Surf., B*, 2018, **170**, 373–381.
9 M. Ma, H. Chen, Y. Chen, X. Wang, F. Chen, X. Cui and J. Shi, *Biomaterials*, 2012, **33**, 989–998.
10 J. You, R. Zhang, G. Zhang, M. Zhong, Y. Liu, C. S. Van Pelt, D. Liang, W. Wei, A. K. Sood and C. Li, *J. Controlled Release*, 2012, **158**, 319–328.

554 | *J. Mater. Chem. B*, 2019, **7**, 548–555

This journal is © The Royal Society of Chemistry 2019

11 B. Liu, C. Li, G. Chen, B. Liu, X. Deng, Y. Wei, J. Xia, B. Xing, P. a. Ma and J. Lin, *Adv. Sci.*, 2017, **4**, 1600540.

12 X. Wang, Y. Ma, H. Chen, X. Wu, H. Qian, X. Yang and Z. Zha, *Colloids Surf., B*, 2017, **152**, 449–458.

13 M. M. Gottesman, T. Fojo and S. E. Bates, *Nat. Rev. Cancer*, 2002, **2**, 48.

14 J. A. Endicott and V. Ling, *Annu. Rev. Biochem.*, 1989, **58**, 137–171.

15 E. M. Leslie, R. G. Deeley and S. P. C. Cole, *Toxicol. Appl. Pharmacol.*, 2005, **204**, 216–237.

16 Y. Fang, Y. Jiang, Y. Zou, F. Meng, J. Zhang, C. Deng, H. Sun and Z. Zhong, *Acta Biomater.*, 2017, **50**, 396–406.

17 A. Cern, D. Marcus, A. Tropsha, Y. Barenholz and A. Goldblum, *J. Controlled Release*, 2017, **252**, 18–27.

18 J. Wen, K. Yang, F. Liu, H. Li, Y. Xu and S. Sun, *Chem. Soc. Rev.*, 2017, **46**, 6024–6045.

19 P. G. Wang, M. Xian, X. Tang, X. Wu, Z. Wen, T. Cai and A. J. Janczuk, *Chem. Rev.*, 2002, **102**, 1091–1134.

20 R. Guo, Y. Tian, Y. Wang and W. Yang, *Adv. Funct. Mater.*, 2017, **27**, 1606398.

21 D. J. Stuehr and M. A. Marletta, *Proc. Natl. Acad. Sci. U. S. A.*, 1985, **82**, 7738–7742.

22 L. A. De, N. Moroni, A. Serafino, A. Primavera, A. Pastore, J. Z. Pedersen, R. Petruzzelli, M. G. Farrace, P. Pierimarchi and G. Moroni, *Biochem. J.*, 2011, **440**, 175–183.

23 C. P. Muir, M. A. Adams and C. H. Graham, *Breast Cancer Res. Treat.*, 2006, **96**, 169–176.

24 W. Xu, L. Z. Liu, M. Loizidou, M. Ahmed and I. G. Charles, *Cell Res.*, 2002, **12**, 311.

25 S. Huerta, S. Chilka and B. Bonavida, *Int. J. Oncol.*, 2008, **33**, 909–927.

26 K. Chegaev, A. Fraix, E. Gazzano, G. E. F. Abd-Ellatef, M. Blangetti, B. Rolando, S. Conoci, C. Riganti, R. Fruttero, A. Gasco and S. Sortino, *ACS Med. Chem. Lett.*, 2017, **8**, 361–365.

27 Z. Du, R. Dou, M. Zu, X. Liu, W. Yin, Y. Zhao, J. Chen, L. Yan and Z. Gu, *Biomater. Sci.*, 2016, **4**, 938–942.

28 J. Fan, N. He, Q. He, Y. Liu, Y. Ma, X. Fu, Y. Liu, P. Huang and X. Chen, *Nanoscale*, 2015, **7**, 20055–20062.

29 M. Guo, H.-J. Xiang, Y. Wang, Q.-L. Zhang, L. An, S.-P. Yang, Y. Ma, Y. Wang and J.-G. Liu, *Chem. Commun.*, 2017, **53**, 3253–3256.

30 L. Tan, A. Wan, X. Zhu and H. Li, *Chem. Commun.*, 2014, **50**, 5725–5728.

31 L. Tan, R. Huang, X. Li, S. Liu and Y.-M. Shen, *Acta Biomater.*, 2017, **57**, 498–510.

32 C.-X. Huang, H.-J. Chen, F. Li, W.-N. Wang, D.-D. Li, X.-Z. Yang, Z.-H. Miao, Z.-B. Zha, Y. Lu and H.-S. Qian, *J. Mater. Chem. B*, 2017, **5**, 9487–9496.

33 X. Wang, Z. Miao, Y. Ma, H. Chen, H. Qian and Z. Zha, *Nanoscale*, 2017, **9**, 14512–14519.

34 H.-J. Xiang, M. Guo, L. An, S.-P. Yang, Q.-L. Zhang and J.-G. Liu, *J. Mater. Chem. B*, 2016, **4**, 4667–4674.

35 B. Deng, P. Ma and Y. Xie, *Nanoscale*, 2015, **7**, 12773–12795.

36 Y. Zhao, C. Zheng, Q. Wang, J. Fang, G. Zhou, H. Zhao, Y. Yang, H. Xu, G. Feng and X. Yang, *Adv. Funct. Mater.*, 2011, **21**, 2035–2042.

37 R. Sultana, D. F. Di, M. Tseng, J. Cai, T. Noel, R. L. Chelvarajan, W. D. Pierce, C. Cini, S. Bondada and D. K. St Clair, *J. Proteome Res.*, 2010, **9**, 6232.

38 Y. Ye, W. P. Li, C. J. Anderson, J. Kao, G. V. Nikiforovich and S. Achilefu, *J. Am. Chem. Soc.*, 2003, **125**, 7766–7767.

39 Y. Deng, L. Huang, H. Yang, H. Ke, H. He, Z. Guo, T. Yang, A. Zhu, H. Wu and H. Chen, *Small*, 2016, **13**.

40 R. Cui, Z. Zhang, J. Nie and B. Du, *Colloid Polym. Sci.*, 2017, **295**, 665–678.

41 L. Ma, Y. Liu, L. Liu, A. Jiang, F. Mao, D. Liu, L. Wang and J. Zhou, *Adv. Funct. Mater.*, 2017, 1705057.

42 Y. Li, Y. Deng, X. Tian, H. Ke, M. Guo, A. Zhu, T. Yang, Z. Guo, Z. Ge, X. Yang and H. Chen, *ACS Nano*, 2015, **9**, 9626–9637.